Photoluminescence enhancement of silicon quantum dot monolayer by plasmonic substrate fabricated by nano-imprint lithography

Hiroto Yanagawa, Asuka Inoue, Hiroshi Sugimoto, Masahiko Shioi, and Minoru Fujii

Citation: Journal of Applied Physics **122**, 223101 (2017);
View online: https://doi.org/10.1063/1.5001106
View Table of Contents: http://aip.scitation.org/toc/jap/122/22
Published by the American Institute of Physics

Photoluminescence enhancement of silicon quantum dot monolayer by plasmonic substrate fabricated by nano-imprint lithography

Hiroto Yanagawa,[1,2] Asuka Inoue,[2] Hiroshi Sugimoto,[2] Masahiko Shioi,[1,2] and Minoru Fujii[2]
[1]*Advanced Research Division, Panasonic Corporation, Seika, Soraku, Kyoto 619-0237, Japan*
[2]*Department of Electrical and Electronic Engineering, Graduate School of Engineering, Kobe University, Rokkodai, Nada, Kobe 657-8501, Japan*

(Received 22 August 2017; accepted 15 November 2017; published online 8 December 2017)

Near-field coupling between a silicon quantum dot (Si-QD) monolayer and a plasmonic substrate fabricated by nano-imprint lithography and having broad multiple resonances in the near-infrared (NIR) window of biological substances was studied by precisely controlling the QDs-substrate distance. A strong enhancement of the NIR photoluminescence (PL) of Si-QDs was observed. Detailed analyses of the PL and PL excitation spectra, the PL decay dynamics, and the reflectance spectra revealed that both the excitation cross-sections and the emission rates are enhanced by the surface plasmon resonances, thanks to the broad multiple resonances of the plasmonic substrate, and that the relative contribution of the two enhancement processes depends strongly on the excitation wavelength. Under excitation by short wavelength photons (405 nm), where enhancement of the excitation cross-section is not expected, the maximum enhancement was obtained when the QDs-substrate distance was around 30 nm. On the other hand, under long wavelength excitation (641 nm), where strong excitation cross-section enhancement is expected, the largest enhancement was obtained when the distance was minimum (around 1 nm). The achievement of efficient excitation of NIR luminescence of Si-QDs by long wavelength photons paves the way for the development of Si-QD-based fluorescence bio-sensing devices with a high bound-to-free ratio. *Published by AIP Publishing.* https://doi.org/10.1063/1.5001106

I. INTRODUCTION

Semiconductor quantum dots (QDs) have several superior properties as near infrared (NIR) phosphors for bio-sensing devices compared to commonly used organic fluorescent dyes,[1] which often suffer from fast fluorescence degradation under light illumination. Fast degradation is a serious obstacle to improve the detection sensitivity of the devices because it limits the excitation power and the accumulation time for detection. Semiconductor QDs, especially Cd and Pb chalcogenide QDs, usually have much more stable luminescence than organic fluorescent dyes, and due to some additional advantages such as the narrow luminescence band, the large tunability of the luminescence wavelength, the broad excitation band, etc., they are considered to be promising candidates for replacing organic fluorescent dyes.[2–6] However, heavy-metal elements in these QDs are always a concern for biomedical applications.[7] As a QD potentially suitable for biomedical applications, Si-QDs have recently been attracting significant attention. For the past decade, the quality of Si-QDs, in particular colloidal solution of Si-QDs, has been improved, and now it is rapidly catching up to that of compound semiconductor QDs.[8–10]

In the application of Si-QDs to bio-sensing devices, a drawback is a small absorption cross-section in the visible and near infrared (NIR) ranges due to the indirect nature of the energy band structure.[11] Since the direct absorption of Si-QDs starts around 400 nm, the efficient excitation requires ultraviolet (UV) light, which degrades biomaterials and also the device sensitivity due to the autofluorescence of biomaterials. To overcome this problem and excite Si-QDs efficiently by long wavelength photons, coupling with surface plasmons supported by metal nanostructures has been proposed.[12–14] A strong enhancement of efficient excitation cross-section of Si-QDs by placing it on a plasmonic substrate has been demonstrated.[15] Furthermore, by tuning the surface plasmon resonance wavelength to the emission wavelength of Si-QDs, Purcell enhancement of the emission rate has been reported.[16–19]

In previous studies on surface plasmon enhanced emission of QDs, metal nanostructures have been produced by several different methods.[20–24] The most widely used process is electron-beam lithography,[12,13,25] which is suitable for the proof-of-concept experiments due to the high accuracy of the fabrication process, although it is very costly. Another often used process is nanosphere lithography,[14,15,18] which uses a two-dimensional array of spheres as a template for the formation of metal nanostructures. Although the process is simple and does not require expensive setups for the formation of metal nanostructures, the freedom of the design, and thus the tunability of the surface plasmon resonance wavelength, is limited. Furthermore, the process usually has a problem in the uniformity and the reproducibility, and is not suitable for the production of commercial devices. A metal film over a nanosphere plasmonic substrate, which uses a spherical array to produce a corrugated metal surface, has the same problem as nanosphere lithography.

In this work, we employ nano-imprint lithography for the fabrication of a plasmonic substrate. The nano-imprint plasmonic substrate has high uniformity in its large area, and the fabrication throughput is very high. Furthermore, the

surface plasmon resonance wavelengths can be controlled easily by the design of the structure. The purpose of this work is to achieve simultaneous enhancement of the excitation cross-section and the emission rate of Si-QDs by placing the monolayer on a properly designed nano-imprint plasmonic substrate, especially under excitation by long wavelength photons suitable for bio-sensing applications. We control the QDs-substrate distance very precisely by using an organic polymer fabricated by a layer-by-layer (LbL) assembly as a spacer. We first characterize the surface plasmon resonance property of the substrate by reflectance spectroscopy. We then study the photoluminescence (PL) and photoluminescence excitation (PLE) spectra and the PL decay dynamics to analyze the relative contributions of the excitation cross-section enhancement and the emission rate enhancement. We also extract the contribution of Purcell enhancement to the total PL enhancement. We show that by the simultaneous enhancement of the excitation cross-section and the emission rate, the PL of a Si-QD monolayer is strongly enhanced under long wavelength excitation exceeding 600 nm.

II. EXPERIMENTAL

We used a colloidal solution of all-inorganic Si-QDs for the formation of a Si-QD monolayer.[26–29] The all-inorganic Si QDs have a heavily B- and P-doped surface layer,[27,28,30,31] which induces negative potential on the surface and prevents the agglomeration in polar solvents by electrostatic repulsions. The Si-QDs can thus be dispersed in water without any organic ligands.[26,27] The Si-QDs exhibit size-tunable and stable luminescence in the visible to NIR ranges in an aqueous solution in a wide pH range.[26,28] Therefore, the all-inorganic Si-QDs are very suitable for bio-photonic applications. The preparation procedure of the Si-QDs can be found in the literature.[26–28,32]

Figure 1(a) shows a photograph of the colloidal dispersion of all-inorganic Si-QDs in methanol. Because of the perfect dispersion of the QDs, the solution is very clear and the characteristic behind the 1 cm^2 cubicle can clearly been read. Figure 1(b) shows the transmission electron microscopy (TEM) (JEOL, JEM-2100 F) image of a Si-QD layer prepared by drop-casting the diluted methanol solution on a carbon-coated Cu mesh. A densely packed monolayer of Si-QDs is formed and no three-dimensional agglomerates are observed. The lattice fringe in the high-resolution image [inset in Fig. 1(b)] corresponds to {1 1 1} planes of the Si crystal. The average size and the standard deviation of the diameter estimated from TEM images are 3.9 nm and 0.8 nm, respectively.[26] Figure 1(c) shows the PL spectra excited at 405 nm and the PLE spectra detected at 850 nm of a Si-QD monolayer on a silica substrate. The Si-QDs exhibit a broad PL around 800 nm. The PL quantum yield (QY) is about 3.9% (see supplementary material for the procedure to determine the QY).[26] The PLE spectrum reveals that the excitation efficiency is very small in the visible range, especially above 600 nm, which is a serious problem for bio-photonic applications.

Figure 1(d) shows a schematic illustration of the structure studied in this work. First, dome-shaped structures were

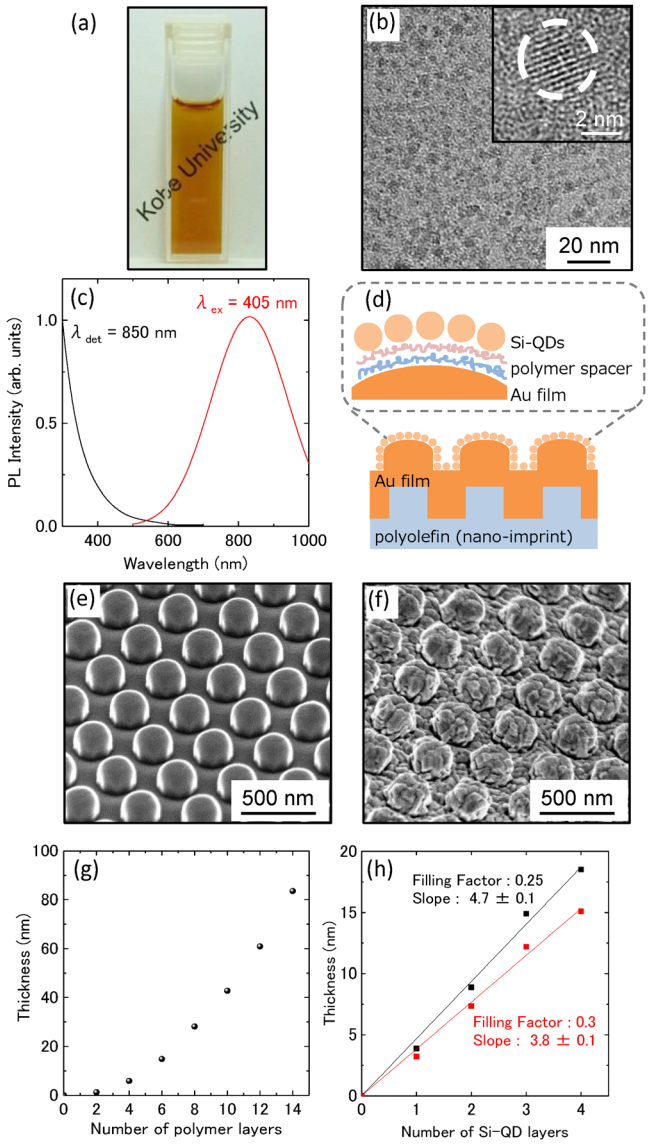

FIG. 1. (a) Photograph of colloidal dispersion of Si-QDs (methanol solution). (b) TEM image of a Si-QD monolayer. The inset shows a high resolution TEM image of a Si-QD. (c) PLE spectrum detected at 850 nm (black) and the PL spectrum excited at 405 nm (red) of a Si-QD monolayer on a silica substrate. (d) Schematic illustration of the cross-section of a nano-imprint plasmonic substrate with a Si-QD monolayer on the surface. SEM image of a polyolefin substrate prepared by nano-imprinting (e) before and (f) after Au deposition. (g) Thickness of the polymer layer on a silica substrate measured by ellipsometry versus the number of polymer layers. (h) Thickness of the Si-QD layer on a silica substrate measured by ellipsometry by assuming the filling factor to be 0.25 and 0.3 versus the number of spin-coating times.

produced on a polyolefin substrate by nano-imprinting. The scanning electron microscopy (SEM) image is shown in Fig. 1(e). The width, the pitch and the height of the dome-shaped structures are 230, 460 and 200 nm, respectively. On the structure, a Au thin film of 300 nm in thickness was deposited by electron-beam evaporation [Fig. 1(f)]. The surface becomes bumpy due to the island growth of Au. For the formation of a Si-QD monolayer on the plasmonic substrate, it was first immersed in an ethanolic solution (1 mM) of 6-amino-1-hexanethiol hydrochloride (6-AHT) for 12 h for the formation of a self-assembled monolayer (SAM) with a positively charged amino group on the surface. A polymer

spacer to control the QDs-substrate distance was then fabricated by the LbL assembly process, i.e., negatively charged [poly(sodium 4-styrenesulfonate) (PSS)] and positively charged [poly(diallyldimethylammonium chloride) (PDDA)] polymers are deposited alternatively by immersing the substrate in the solutions (supplementary material).[33–35] Figure 1(g) shows the thickness of the polymer layers estimated by spectroscopic ellipsometry (HORIBA, Auto-SE) as a function of the layer number. The refractive indices of PDDA and PSS layers are 1.41 and 1.50, respectively.[36] The thickness is controlled from 1 nm to 84 nm by changing the layer number from 0 to 14. Finally, a monolayer of Si-QDs was formed on the positively charged surface by spin coating a diluted colloidal solution of Si-QDs (0.2 mg/ml) (500 rpm for 5 s followed by 1500 rpm for 30 s). The formation of a monolayer was confirmed by measuring the thickness of the layer deposited on a flat substrate by spectroscopic ellipsometry (supplementary material). In Fig. 1(h), the thickness of Si-QD layers on a flat Au film is plotted as a function of the number of spin coats (supplementary material). For the estimation of the thickness, an effective medium approximation was used as the dielectric permittivity of a Si-QD layer by assuming the filling factor to be 0.25 or 0.3. The thickness increases linearly with the slopes of 3.8 nm/layer and 4.7 nm/layer for the filling factors of 0.3 and 0.25, respectively. These values are very close to the average diameter of Si-QDs (3.9 nm in diameter), and thus nearly a monolayer of Si-QDs is formed by one spin coating process.

The fabricated structures are characterized by reflectance spectroscopy. The reflectance spectra were measured in a wide wavelength range (180 nm–1600 nm) with the incident angle of 45° or 60° by a UV-Vis-NIR spectrophotometer (Shimadzu, SolidSpec-3700). PL and PLE spectra were measured by a stand-alone spectrophotometer equipped with a Xe lamp and a double monochromator as an excitation source (HORIBA, Fluorolog-3). PL spectra were also excited by 405 nm or 641 nm semiconductor lasers (COHERENT, CUBE). PL decay curves were obtained by using a single spectrometer equipped with an image intensified CCD (Roper Scientific, PI-Max1024HB). The excitation source was modulated with 405 nm light. The measurement geometries are shown in the supplementary material.

III. RESULTS AND DISCUSSION

Figure 2 shows the specular reflectance spectra of plasmonic substrates with different thicknesses of polymer layers and a Si-QD monolayer. The incident angle is 45°. The data obtained with the incident angle of 60° are shown in the supplementary material (Fig. S2). The number of polymer layers ($L(n)$) is changed from 0 to 14. In the sample without a polymer layer ($L(0)$), i.e., a plasmonic substrate with a Si-QD monolayer directly on it, the reflectance dips are observed in three wavelength ranges. The reflection loss below 500 nm is due to the interband transitions of Au, and does not contribute to the luminescence enhancement of Si-QDs. The narrow dip around 650 nm and the broad one around 800 nm are due to the excitation of surface plasmons. The 800 nm band overlaps well with the emission band of Si-QDs in Fig. 1(c), and

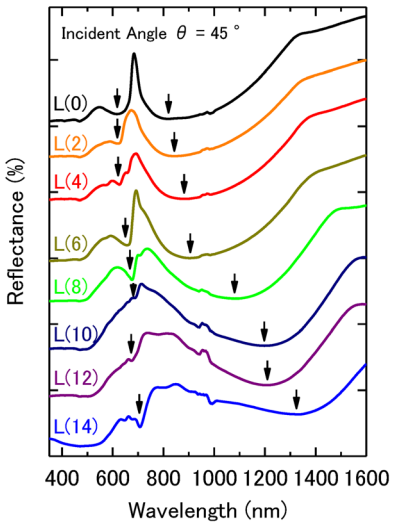

FIG. 2. Reflectance spectra of Si-QD monolayer/plasmonic substrate structures. The number of spacer layers is changed from 0 to 14. The incident angle is 45°.

thus strong enhancement of the emission rate is expected by coupling with the mode. On the other hand, the 650 nm band can be used for the enhancement of the excitation cross-section, if we chose the wavelength for the excitation of Si-QDs. The reflectance spectrum depends strongly on the number of polymer layers. The dip around 650 nm slightly shifts to longer wavelengths with increasing polymer thickness. On the other hand, the broad dip around 800 nm shifts significantly to longer wavelengths with increasing thickness and reaches around 1300 nm in $L(14)$. The long wavelength shift is explained by the increased permittivity around Au nanostructures. The high sensitivity of the long wavelength mode to the dielectric environment suggests that the mode is a dipolar mode. On the other hand, the mode around 650 nm can be assigned to a quadrupolar mode.

Figure 3(a) shows the PLE spectra detected at 850 nm. The bandwidth of the detection is about 15 nm. As references, the PLE spectrum of a Si-QD monolayer on a silica substrate and that on a Au flat film are also shown. Note that the ordinate is a logarithmic scale. On a silica substrate, the intensity decreases monotonously to longer wavelengths and the data become noisy above 500 nm. The intensity becomes much small on a Au flat film and no reliable data are obtained above 500 nm. This is due to non-radiative relaxation of excited Si-QDs to lossy surface modes and surface plasmon polaritons of a Au flat film. On plasmonic substrates, the shape of the PLE spectrum is strongly modified and the intensity increases compared to that on a silica substrate, especially above 500 nm. In order to quantitatively analyze the change in the PLE spectral shape, we divided the PLE spectra of a Si-QD monolayer on plasmonic substrates by that on a silica substrate and obtained the PLE enhancement factor spectra [Fig. 3(b)] (see supplementary material for the procedure). In Fig. 3(b), we can see that the PL excitation efficiency is strongly enhanced, especially above 500 nm.

In Fig. 3(c), the PLE enhancement factor spectrum of $L(0)$ is compared with the reflectance spectrum. The strong enhancement around 650 nm coincides very well with the

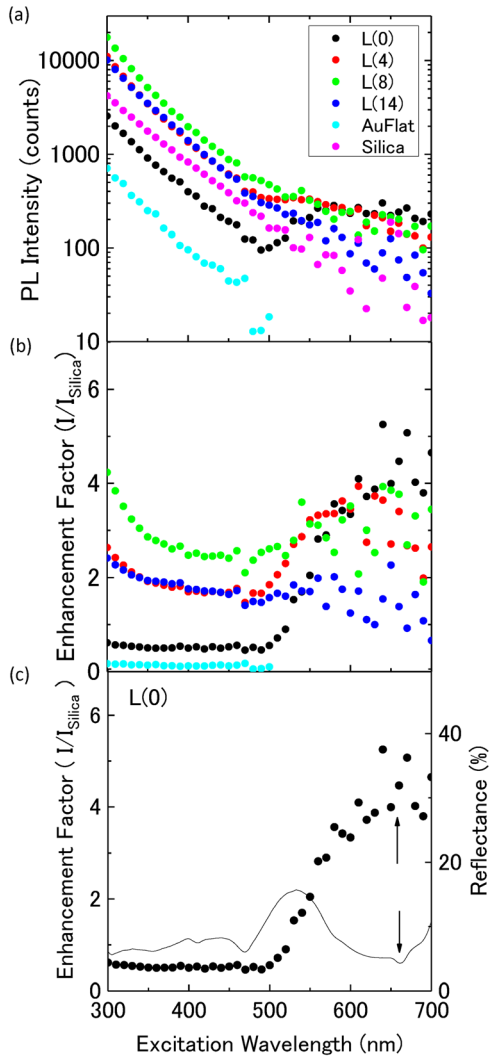

FIG. 3. (a) PLE spectra of Si-QD monolayer/plasmonic substrate structures detected at 850 nm. The number of spacer layers is changed from 0 to 14. The data for a Si-QD monolayer on a silica substrate (Silica) and on a Au flat film (AuFlat) are also shown. (b) PLE enhancement factor spectra obtained by dividing the PLE spectra of Si-QD monolayer/plasmonic substrate structures by that of a Si-QD monolayer on a silica substrate. (c) Comparison of the enhancement factor spectra for $L(0)$ and the reflectance spectrum (line) measured with the incident angle of 60°.

reflection loss designated by an arrow. This indicates that the PL enhancement in the excitation wavelength range is due to the enhancement of the excitation cross-section induced by enhanced electric fields of surface plasmons supported by Au nanostructures. Similar data for other polymer thicknesses are summarized in the supplementary material (Fig. S3).

Figure 4(a) shows the PL spectra excited at 405 nm. As references, the spectra on a silica substrate and on a Au flat film are shown. On plasmonic substrates, the PL is strongly enhanced. The maximum enhancement factor reaches over 10 in $L(8)$. Furthermore, the spectral shape is strongly modified, especially in $L(14)$. Figure 4(b) shows the PL enhancement factor obtained by dividing the PL spectra of the samples with that on a silica substrate. The enhancement factor spectrum depends strongly on the polymer thickness. In Figs. 4(c)–4(f), the PL enhancement factor spectra of $L(0)$, $L(4)$, $L(8)$ and $L(14)$, respectively, are compared with the reflectance spectra. The peak of the enhancement factor spectra coincides fairly well with the dip in the reflectance spectra. Therefore, the strong modification of the spectral shape is caused by the modification of the emission rate of Si-QDs due to the coupling with surface plasmons in the plasmonic substrates.[37] Similar data obtained for 641 nm excitations are summarized in the supplementary material (Fig. S4).

In Fig. 4(g), the PL enhancement factor at 850 nm is plotted as a function of the polymer layer number for 405 and 641 nm excitations. Under 405 nm excitation, the PL enhancement factor increases with increasing layer number, reaches a maximum at $L(8)$ (9-fold) and then decreases. On the other hand, under 641 nm excitation, the enhancement factor is the largest (22-fold) at $L(0)$ and monotonously

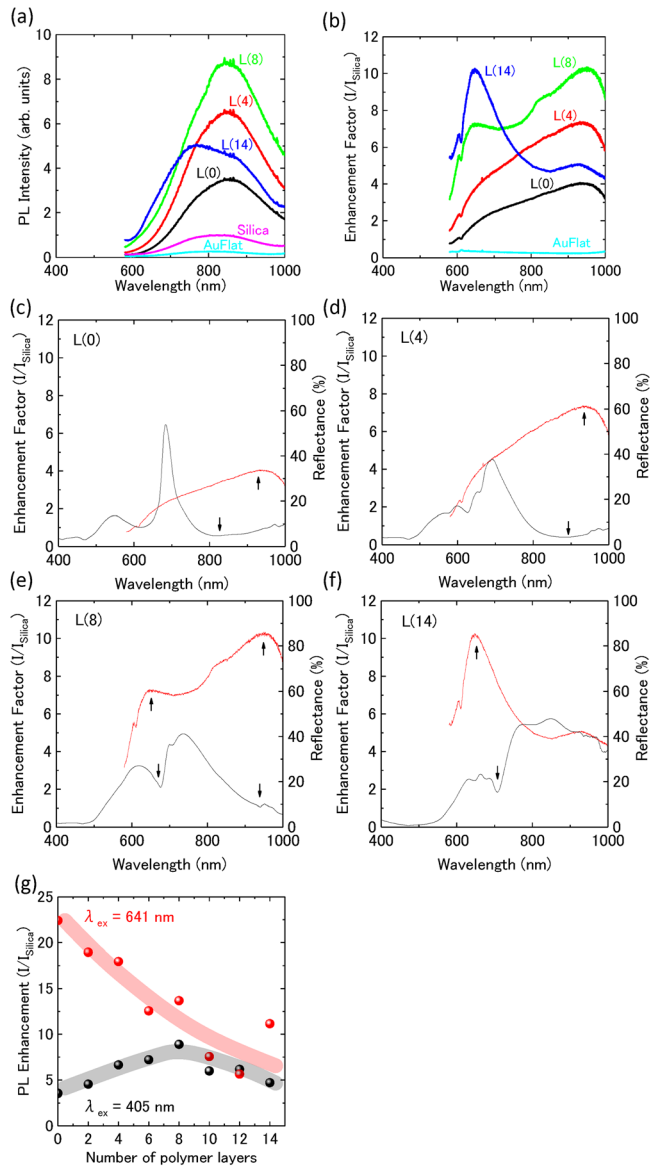

FIG. 4. (a) PL spectra of Si-QD monolayer/plasmonic substrate structures excited at 405 nm. The number of spacer layers is changed from 0 to 14. The data for a Si-QD monolayer on a silica substrate and on a Au flat film are also shown. (b) PL enhancement factor spectra obtained by dividing the PL spectra of Si-QD monolayer/plasmonic substrate structures by that of a Si-QD monolayer on a silica substrate. Comparison of PL enhancement factor spectra (red) and reflectance spectra (black) for (c) $L(0)$, (d) $L(4)$, (e) $L(8)$ and (f) $L(14)$. (g) PL enhancement factor at 850 nm versus the number of polymer layers under excitation at 405 nm (black) and 641 nm (red).

decreases with increasing layer number. The different behavior between the two excitation wavelengths indicates that the enhancement mechanism is different. Under 405 nm excitation, the enhancement of the excitation process is not expected because of the large imaginary part of the dielectric constant. The PL enhancement is thus solely due to the enhancement of the quantum efficiency arising from the large antenna efficiency. It is well known that the antenna efficiency has an optimal distance due to the competition between the radiative rate enhancement and the dissipation to lossy modes.[38] In the present structure, the optimum distance seems to be around 30 nm. On the other hand, under 641 nm excitation, in addition to the quantum efficiency enhancement, the enhancement of the excitation efficiency plays an important role. The excitation efficiency enhancement due to the enhanced incident electric field is the largest on the surface of metal nanostructures. The monotonous decrease of the enhancement factor with increasing polymer thickness indicates that the excitation efficiency enhancement is dominant under 641 nm excitation.

Figure 5(a) shows PL decay curves detected in the range of 800 nm to 850 nm. The excitation wavelength is 405 nm. The decay curves are non-exponential as has been commonly observed in Si-QD ensembles. In Fig. 5(b), the decay rate, $\Gamma = 1/\tau_{ave}$, where τ_{ave} is the average PL lifetime, is plotted as a function of a detection wavelength. To estimate the average lifetime, the decay curves are fitted by a stretched exponential function, $I = I_0 \exp\{(-t/\tau)^{\beta}\}$, where τ is the decay constant and β is the stretching parameter. The average PL lifetime (τ_{ave}) is defined as $\tau_{ave} = \tau\beta^{-1}\Gamma_E(\beta^{-1})$, where Γ_E is the Euler gamma function. On silica, the decay rate is 0.1–0.4 μs^{-1} in the wavelength range. The larger decay rate at shorter wavelengths is usually explained by the better overlap of electron and hole wavefunctions in the momentum space in smaller QDs. The decay rate is enhanced both on a Au flat film and on plasmonic substrates.[39] Within the data on the plasmonic substrates, the decay rate is the largest in $L(0)$ and becomes small with increasing distance. This can be seen more clearly in the enhancement factor of the decay rates, which is defined by the ratio of the decay rates to that of a Si-QD monolayer on a silica substrate [Fig. 5(c)].

In Fig. 5(c), the decay rate enhancement arises both from the Purcell enhancement (radiative rate enhancement), which contributes to the enhancement of the quantum efficiency and the dissipation to lossy modes.[40] We extract the Purcell enhancement factor (P/P_{Silica}), where P is the Purcell factor of a sample and P_{Silica} is that of a Si-QD monolayer on a silica substrate, from the enhancement factors of the decay rate (Γ_{Silica}/Γ) and the intensity (I/I_{Silica}) by the following procedure. The enhancement factor of the PL intensity is expressed as $I/I_{Silica} = Q/Q_{Silica} \cdot \sigma/\sigma_{Silica} \cdot \eta/\eta_{Silica}$, where Q is the quantum efficiency, σ is the excitation cross-section and η is the light collection efficiency. The quantum efficiency enhancement factor (Q/Q_{Silica}) is $Q/Q_{Silica} = P/P_{Silica} \cdot \Gamma_{Silica}/\Gamma$. Among these parameters, the excitation cross-section ratio (σ/σ_{Silica}) can be approximated to be unity under 405 nm excitation. On the other hand, the collection efficiency is largely different, because substantial amounts of photons are emitted onto the substrate side and cannot be collected in a Si-QD monolayer on a silica substrate. In the case of a dipole emitter placed on a silica substrate with the refractive index of 1.45,

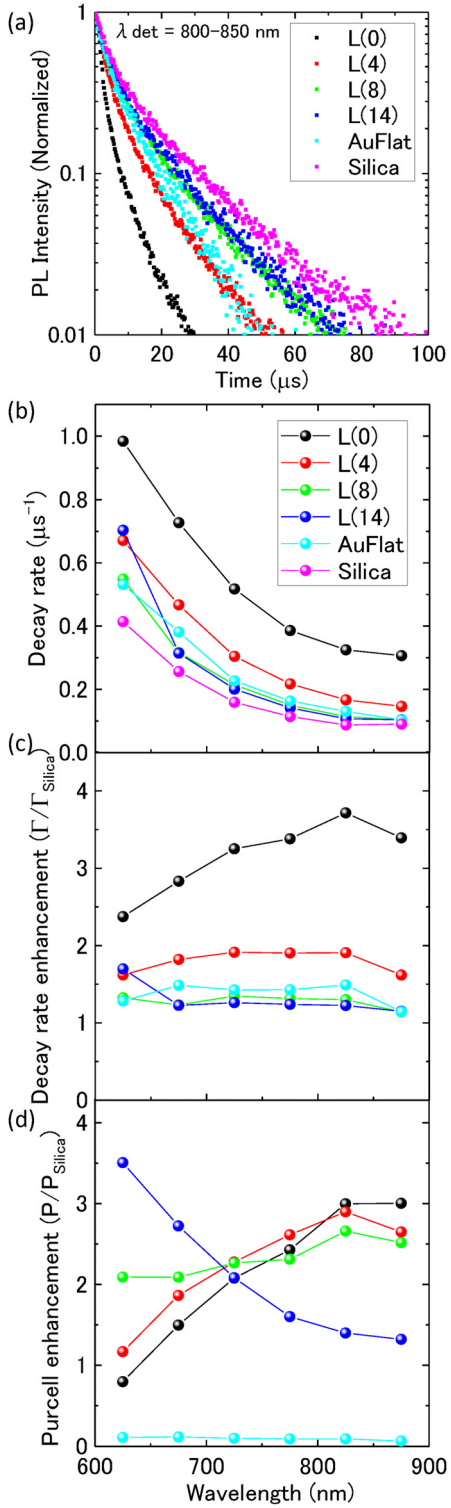

FIG. 5. (a) PL decay curves of Si-QD monolayer/plasmonic substrate structures excited at 405 nm. The number of spacer layers is changed from 0 to 14. The detection wavelength is in the range of 800 nm to 850 nm. (b) PL decay rates obtained from the decay curves as a function of detection wavelength. (c) Decay rate enhancement factor obtained by dividing the decay rates of Si-QD monolayer/plasmonic substrate structures by that of a Si-QD monolayer on a silica substrate. (d) Enhancement factor of Purcell factors as a function of detection wavelength.

about 24% of photons are emitted upward and others onto the substrate. Therefore, η/η_{Silica} becomes about 1/0.24, and I/I_{Silica} is approximated to $P/P_{Silica} \cdot \Gamma_{Silica}/\Gamma \cdot 1/0.24$. Figure 5(d) shows the Purcell factor enhancement as a function of the detection wavelength. As is expected, on a Au flat film, no Purcell enhancement can be seen. On plasmonic substrates, the Purcell factor is strongly enhanced. The Purcell factor enhancements of $L(0)$ and $L(4)$ have similar wavelength dependence and are larger at longer wavelengths. This suggests that the enhancement is due to the coupling with the longer wavelength surface plasmon mode in Fig. 2. The wavelength dependence becomes small in $L(8)$ and the dependence is reversed in $L(14)$. This can be explained by the fact that the longer wavelength mode shifts beyond the emission wavelength and the enhancement is mainly from the coupling with the shorter wavelength surface plasmon mode in $L(14)$.

IV. CONCLUSION

We have prepared a plasmonic substrate suitable for the excitation of NIR luminescence of Si-QDs by long wavelength photons for bio-sensing applications by using nanoimprint lithography. The reflectance spectra revealed that the plasmonic substrates have two surface plasmon bands, which can be used for excitation and emission enhancements. We placed a monolayer of Si-QDs on the plasmonic substrate by controlling the QDs-substrate distance precisely by polymer spacers. PL and PLE spectra and the decay characteristics in combination with the reflectance spectra revealed that both the excitation and emission processes of Si-QDs are strongly modified by the plasmonic substrate. In particular, under 641 nm excitation, the excitation efficiency was largely enhanced. The efficient excitation of NIR PL of Si-QDs by long wavelength photons is an important achievement for the application of Si-QDs in bio-sensing devices, because autofluorescence of bio-materials can be suppressed significantly compared to the case of UV excitation.

SUPPLEMENTARY MATERIAL

See supplementary material for the procedure to determine the QY of Si-QDs, the formation method of a polymer spacer by the LbL assembly process, the estimation of the thickness of the Si-QD monolayer by ellipsometry, the measurement geometry of PL and PLE, reflectance spectra of Si-QDs on a plasmonic substrate at an incident angle of 60°, the PLE enhancement factor spectra of a Si-QD/L(n)/plasmonic substrate and the reflectance spectra, the PL spectra and PL enhancement factor spectra of a Si-QD monolayer excited at 405 and 641 nm, and the PL decay curves of a Si-QD monolayer.

ACKNOWLEDGMENTS

This work was partly supported by the 2015 JST Visegrad Group (V4)-Japan Joint Research Project on Advanced Materials and a JSPS KAKENHI Grant No. 16H03828.

[1]U. Resch-Genger, M. Grabolle, S. Cavaliere-Jaricot, R. Nitschke, and T. Nann, Nat. Methods **5**, 763 (2008).
[2]W. C. Chan, Science **281**, 2016 (1998).
[3]X. Michalet, Science **307**, 538 (2005).
[4]I. L. Medintz, H. T. Uyeda, E. R. Goldman, and H. Mattoussi, Nat. Mater. **4**, 435 (2005).
[5]M. Bruchez, M. Moronne, P. Gin, S. Weiss, and A. P. Alivisatos, Science **281**, 2013 (1998).
[6]W. C. Chan, D. J. Maxwell, X. Gao, R. E. Bailey, M. Han, and S. Nie, Curr. Opin. Biotechnol. **13**, 40 (2002).
[7]K. M. Tsoi, Q. Dai, B. A. Alman, and W. C. W. Chan, Acc. Chem. Res. **46**, 662 (2013).
[8]M. Dasog, G. B. De los Reyes, L. V. Titova, F. A. Hegmann, and J. G. C. Veinot, ACS Nano **8**, 9636 (2014).
[9]M. L. Mastronardi, F. Maier-Flaig, D. Faulkner, E. J. Henderson, C. Kübel, U. Lemmer, and G. A. Ozin, Nano Lett. **12**, 337 (2012).
[10]F. Sangghaleh, I. Sychugov, Z. Yang, J. G. C. Veinot, and J. Linnros, ACS Nano **9**, 7097 (2015).
[11]W. L. Wilson, P. F. Szajowski, and L. E. Brus, Science **262**, 1242 (1993).
[12]J. S. Biteen, D. Pacifici, N. S. Lewis, and H. A. Atwater, Nano Lett. **5**, 1768 (2005).
[13]J. S. Biteen, N. S. Lewis, H. A. Atwater, H. Mertens, and A. Polman, Appl. Phys. Lett. **88**, 131109 (2006).
[14]Y. Mochizuki, M. Fujii, S. Hayashi, T. Tsuruoka, and K. Akamatsu, J. Appl. Phys. **106**, 13517 (2009).
[15]A. Inoue, H. Sugimoto, and M. Fujii, J. Phys. Chem. C **121**, 11609 (2017).
[16]E. Takeda, M. Fujii, T. Nakamura, Y. Mochizuki, and S. Hayashi, J. Appl. Phys. **102**, 23506 (2007).
[17]K. Imakita, M. Fujii, T. Nakamura, S. Miura, E. Takeda, and S. Hayashi, Jpn. J. Appl. Phys., Part 1 **45**, 6132 (2006).
[18]H. Sugimoto, S. Yashima, K. Furuta, A. Inoue, and M. Fujii, Appl. Phys. Lett. **108**, 241103 (2016).
[19]J. S. Biteen, L. A. Sweatlock, H. Mertens, N. S. Lewis, A. Polman, and H. A. Atwater, J. Phys. Chem. C **111**, 13372 (2007).
[20]J. Song, T. Atay, S. Shi, H. Urabe, and A. V. Nurmikko, Nano Lett. **5**, 1557 (2005).
[21]K. T. Shimizu, W. K. Woo, B. R. Fisher, H. J. Eisler, and M. G. Bawendi, Phys. Rev. Lett. **89**, 117401 (2002).
[22]J. Zhang, Y. H. Ye, X. Wang, P. Rochon, and M. Xiao, Phys. Rev. B **72**, 201306(R) (2005).
[23]A. G. Brolo, S. C. Kwok, M. D. Cooper, M. G. Moffitt, C. W. Wang, R. Gordon, J. Riordon, and K. L. Kavanagh, J. Phys. Chem. B **110**, 8307 (2006).
[24]S.-J. Park, S.-W. Lee, S. Jeong, J.-H. Lee, H.-H. Park, D.-G. Choi, J.-H. Jeong, and J.-H. Choi, Nanoscale Res. Lett. **5**, 1590 (2010).
[25]P. P. Pompa, L. Martiradonna, A. D. Torre, F. D. Sala, L. Manna, M. De Vittorio, F. Calabi, R. Cingolani, and R. Rinaldi, Nat. Nanotechnol. **9**, 723 (2014).
[26]H. Sugimoto, M. Fujii, Y. Fukuda, K. Imakita, and K. Akamatsu, Nanoscale **6**, 122 (2014).
[27]H. Sugimoto, M. Fujii, K. Imakita, S. Hayashi, and K. Akamatsu, J. Phys. Chem. C **116**, 17969 (2012).
[28]H. Sugimoto, M. Fujii, K. Imakita, S. Hayashi, and K. Akamatsu, J. Phys. Chem. C **117**, 11850 (2013).
[29]M. Fujii, H. Sugimoto, and K. Imakita, Nanotechnology **27**, 262001 (2016).
[30]M. Fujii, H. Sugimoto, M. Hasegawa, and K. Imakita, J. Appl. Phys. **115**, 84301 (2014).
[31]K. Nomoto, H. Sugimoto, A. Breen, A. V. Ceguerra, T. Kanno, S. P. Ringer, I. P. Wurfl, G. Conibeer, and M. Fujii, J. Phys. Chem. C **120**, 17845 (2016).
[32]M. Fukuda, M. Fujii, H. Sugimoto, K. Imakita, and S. Hayashi, Opt. Lett. **36**, 4026 (2011).
[33]O. Kulakovich, N. Strekal, A. Yaroshevich, S. Maskevich, S. Gaponenko, I. Nabiev, U. Woggon, and M. Artemyev, Nano Lett. **2**, 1449 (2002).
[34]Y.-H. Chan, J. Chen, S. E. Wark, S. L. Skiles, D. H. Son, and J. D. Batteas, ACS Nano **3**, 1735 (2009).
[35]Q. Cui, F. He, L. Li, and H. Möhwald, Adv. Colloid Interface Sci. **207**, 164 (2014).
[36]C. Ma, M. P. Srinivasan, A. J. Waring, R. I. Lehrer, M. L. Longo, and P. Stroeve, Colloids Surf., B **28**, 319 (2003).
[37]M. Ramezani, G. Lozano, M. A. Verschuuren, and J. Gómez-Rivas, Phys. Rev. B **94**, 125406 (2016).
[38]P. Anger, P. Bharadwaj, and L. Novotny, Phys. Rev. Lett. **96**, 113002 (2006).
[39]R. Guo, S. Derom, A. I. Väkeväinen, R. J. A. van Dijk-Moes, P. Liljeroth, D. Vanmaekelbergh, and P. Törmä, Opt. Express **23**, 28206 (2015).
[40]G. Lozano, D. J. Louwers, S. R. Rodríguez, S. Murai, O. T. Jansen, M. A. Verschuuren, and J. Gómez Rivas, Light: Sci. Appl. **2**, e66 (2013).